JOURNAL OF MATERIALS SCIENCE 1 (1966) 317–335

Superconductivity in Deformed Niobium Alloys

A. V. NARLIKAR, D. DEW-HUGHES
Department of Physics, The University, Lancaster, UK

Received 27 May 1966

A brief review of deformation structure in bcc metals is given and the main features of type II superconductivity are summarised. Microstructure and superconducting properties of deformed niobium-tantalum, niobium-titanium, and niobium-zirconium alloys were studied and compared with those of pure niobium. All these alloys are type II superconductors, which above a certain critical field, H_{c_1}, enter the mixed state, consisting of Abrikosov current vortices in a superconducting matrix. Dislocations introduced by deformation interact with current vortices to cause irreversible superconducting behaviour and contribute to a high current-carrying capacity. It is concluded from the results presented here that a strong vortex dislocation interaction is obtained only when a non-uniform dislocation distribution is present, and that a uniform distribution produces only weak pinning. Flux-pinning by dislocation tangles is treated as a special case of pinning by normal particles resulting from a variation in κ, the Ginzburg-Landau parameter.

1. Introduction

Three superconducting materials are currently available commercially for the construction of electromagnets for generating fields in the range 50 to 100 kOe. Of these, the intermetallic compound Nb_3Sn is brittle and cannot be deformed. The other two are alloys of Nb-Zr and Nb-Ti, and their superconducting properties, in particular current-carrying capacity, are vastly enhanced by cold-work. This improvement in properties has been attributed to the introduction of a high density of dislocations during plastic deformation. The aim of this investigation was an unambiguous determination of the role of dislocations in these high-field superconductors.

High-field superconductors have been thoroughly discussed in three recent review articles [1-3], but a brief résumé of the salient features is desirable here. An ideal, or type I, superconductor may be driven normal below its critical temperature by the application of a magnetic field exceeding a critical value, H_c, for that temperature. Below H_c, the magnetic field is completely excluded from the bulk of a superconductor. Critical fields are generally low (500 Oe or less) and, because of the self-field from any current flowing in the superconductor, a critical current exists which is also low. There is a dimensionless parameter of the Ginzburg-Landau theory [4], κ, which is related to ρ_n, the electrical resistivity of the material in the normal state [5]:

$$\kappa = \kappa_0 + 7.5 \times 10^{-6} (\gamma)^{\frac{1}{2}} \rho_n \qquad (1)$$

κ_0 is a constant of the pure superconductor, and γ is the temperature coefficient of the electronic specific heat. κ typically has a value of 0.1 for a pure, type I superconductor. Should κ be greater than $1/\sqrt{2}$ ($= 0.707$), the superconductor changes its behaviour in a magnetic field, and becomes what is known as type II. Alloying, by increasing ρ_n, will increase κ, and most concentrated (i.e. more than a few at. %) alloys are type II. Pure Nb and, possibly, V are the only elements which show type II behaviour. A type II superconductor behaves just like a type I up to a magnetic field H_{c_1}, which is below the critical field for the material. At H_{c_1}, the magnetic field begins to penetrate the superconductor; this penetration is incomplete, and the material remains super-

conducting, until a much higher field, H_{c2}. For the Nb alloys investigated, H_{c2} may be as high as 100 kOe; this is to be compared with 2500 Oe for pure Nb and 500 Oe for pure Pb, a type I material.

At fields between H_{c1} and H_{c2}, the superconductor is in the "mixed state". Abrikosov [6] has shown that the mixed state consists of a structure of quantised supercurrent vortices, each carrying a quantum of flux $\phi_0 = hc/2e$ ($= 2 \times 10^{-7}$ gauss/cm^2). These may be represented as a core or filament of normal material embedded in a superconducting matrix. As the field is increased, the density of these vortices increases until they are so close together that their cores begin to overlap; this point being H_{c2}. Fig. 1 is a schematic representation of the magnetisation curve as calculated by Abrikosov for a superconductor with $\kappa \gg 1$, compared to that for a type I superconductor (also shown is an irreversible curve).

The pure, reversible, Abrikosov mixed state is, however, not able to carry current without resistance (except for a surface current). One

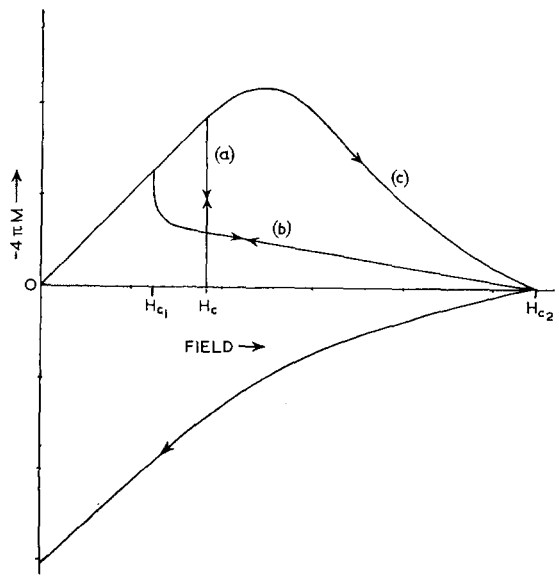

Figure 1 Schematic magnetisation curves of superconductors: (a) type I; (b) reversible type II; (c) irreversible type II.

of Maxwell's equations gives $4\pi J = \text{curl } H$; a current density J will result in a non-uniform field H. A current flowing in the mixed state will give rise to a non-uniform distribution of supercurrent flux vortices. Because of their mutual repulsion, such a distribution would be unstable. Evetts [7] has shown that a simple vortex in a non-uniform array experiences a force per unit length $1/4\pi\ (\hat{\phi}_0/|\phi_0|) \wedge \text{curl } H_A\hat{\phi}_0$, where $\hat{\phi}_0$ is a vector directed along the flux line, and H_A is the field which, according to the Abrikosov theory, would be in equilibrium with the local value of magnetic induction in the neighbourhood of the flux line. This formula takes into account the Lorentz force and any line tension effects of a curved vortex line. Under the action of this force, the vortices would move. One can take a very simple view that in doing so they reduce curl H and hence J. It has been suggested that moving vortices (which have magnetic flux associated with them) crossing a current will give rise to a resistance [8, 9]. This idea has met with several objections [10, 11], and has also been hotly defended [12-14]. Once a resistance is generated, the material is, of course, no longer superconducting and is of no practical interest.

The exact mechanism whereby the motion of vortices gives rise to a resistance (actually to an induced electric field) is in doubt, but that it must do so can be seen as follows [15]. The time-dependent Ginzburg-Landau theory has not yet been solved, and it is not known if the flux vortices retain their identity when in motion. It is necessary then to consider a frame of reference moving with the velocity v of the vortices. In this frame, the vortices are stationary, and exist as predicted by Abrikosov. The lattice of the superconductor is moving past them with a velocity v_x in the x direction, but it is assumed that any interaction with a perfect lattice is negligible. As in this frame of reference the material is in the mixed state, uncomplicated by flux motion, the material remains superconducting and the electric field is everywhere zero. The transformation equations, back to the laboratory frame, give*

$$E_y' = E_y - \frac{v_x H_z}{c} \qquad (2)$$

(as v_x is small compared to c, the relativistic coefficient is neglected). But E_y', the field in the moving frame, is zero, so there is a field E_y in the laboratory frame equal to $(v_x/c)\,H_z$, where H_z is the magnetic field in the z direction; the current is flowing in the y direction. Inverting Ohm's law, $E_y = \rho J_y$, and hence the induced resistivity

* See, for example, W. H. McCrea, *Relativity Physics* (Methuen, 1935).

$$\rho = \frac{v_x H_z}{c J_y} \qquad (3)$$

The velocity of flux vortices has been shown to be from 300 to 3000 cm/sec [16, 17]. For a highly reversible superconductor, the critical current density may be 10 A/cm^2 at 1000 Oe [18]. Substituting these values in the above equation yields a resistivity of 10^{-6} to 10^{-5} ohm cm, which is the expected range of values for the normal state resistivity of an alloy at 4.2° K.

Clearly, to carry high currents without resistance, it is necessary to prevent the motion of flux lines. Inhomogeneities must be introduced into the lattice which will interact with the flux vortices and resist the driving force on the vortices. When this is done, the superconducting properties become irreversible; the magnetisation curve is as the irreversible curve shown in fig. 1. The superconductor is now said to be in the critical state; everywhere, the flux gradient is such that the driving force is just balanced by the pinning interaction. The degree of hysteresis in the magnetisation curve may be related to the current-carrying capacity, and is a useful measure of the degree of success one achieves in improving the superconducting properties. The introduction of dislocations is one way in which the lattice may be modified to interact with flux lines. The experiments described in this paper were designed to elucidate the nature of that interaction.

The effect of deformation on superconducting properties has been studied recently by several workers, and it is found that the current-carrying capacity and the magnetic hysteresis of the specimen are enhanced after deformation [19-22]. However, only a very few attempts have been made to relate the results of these measurements with the microstructure. Walker *et al* [23] attempted to explain the observed anisotropy in the measured values of critical currents in the Nb-Zr alloy specimens in terms of the anisotropy in the dislocation structure, while Catterall and Williams [24] studied the variation in magnetisation and critical currents in heat-treated Nb specimens in relation to the resulting microstructure. The earlier work of Narlikar and Dew-Hughes [25] had suggested that the dislocation cell walls in deformed Nb and V are chiefly responsible for flux pinning. The results of these studies have already been discussed in the review articles mentioned above [1-3]; the effect of dislocations on superconducting properties has also been the subject of a separate review [26]. This paper describes the results of more extensive studies of the microstructure and superconducting properties than those reported in reference 25. The materials studied were single and polycrystalline pure Nb, Nb-50 at. % Ta, Nb-25 at. % Ti and Nb-25 at. % Zr alloys.

2. Survey of Deformation Structure in bcc Metals

The deformation structure in bcc metals has not been studied as extensively as in fcc metals. However, during the last few years a wealth of information has been obtained regarding their deformation behaviour. Many bcc metals, such as α-Fe [27-29], Nb [30-32], Ta [33, 34], V [35, 36], Mo [37] and W [38-40], have been investigated recently, and their microstructure studied by transmission electron microscopy. Very little information is available in the literature regarding the deformation structure in any of the alloys of these metals, but recently some work on the structure and mechanical properties of Ta-Mo alloy crystals has been reported [41].

The deformation structure in pure bcc metals is found to depend upon several factors, such as the amount of strain, the temperature of deformation, etc. When pure, bcc metals have high stacking-fault energies, and the dislocation structure observed in deformed metals is found to resemble that observed in fcc metals of high stacking-fault energy. The results of transmission electron microscopic studies of the deformation structures observed in bcc metals may be summarised in the following points.

(a) During early stages of deformation, the dislocations are jogged; dipoles and elongated dislocation loops are observed. As the strain is increased, the dislocations tend to cluster together to form *tangles*. On increasing the strain further, the tangles begin to join up and finally a *cell structure* is formed. The cell walls are made up of tangles of dislocations with high density, while there are relatively few dislocations present within each cell.

(b) The average cell size decreases rapidly during the early stage of deformation and then reaches a constant value. The misorientation across the cell walls and the dislocation density in them, however, increase with deformation.

(c) The average dislocation density in deformed metals is found to be 3 to 5 times smaller than

in the cell walls. The dislocation density is found to depend upon the grain size; the smaller the grain size, the greater is the dislocation density. On the other hand, it is found to be independent of the deformation temperature so long as the latter is below the temperature at which recovery commences.

2.1. The Cell Structure

Transmission electron microscopic studies of bcc metals began at a much later date than for fcc metals. The very first transmission electron microscopic studies of Heidenreich [42] in 1949 had revealed that the grains of deformed Al are broken up into small domains or cells, 1 to 2 μm in diameter. However, more thorough investigation began only in 1956, by which time electron microscopy and specimen preparation were developed into standard metallographic techniques. The subsequent studies of a number of pure metals and alloys revealed the almost universal presence of a cell structure.

The existence of a cell structure in crystals was in fact perceived long before electron microscopic observations were made. In 1922, Darwin [43], in order to explain the observed intensities of X-ray reflections from crystals, was led to the idea that real crystals are imperfect, being made of mosaics of perfect crystal blocks misoriented through small angles. The existence of these mosaic blocks was soon demonstrated by a number of workers [44-46]. However, no satisfactory model of an imperfect crystal existed until 1934. Two main models were proposed. In Smekal's model [47], the imperfections were believed to be introduced accidentally either during crystal growth or during subsequent deformation. On the other hand, theoretical considerations led Zwicky [48] to the idea that a perfect crystal was energetically unstable as compared to an imperfect one. Zwicky's calculations were later, however, found to be erroneous and no experimental observations were made to support his model.

A real advance in the description of imperfect crystals was made only when the concept of dislocations was introduced. With the work of Bragg [49] and of Burgers [50], it became clear that the mosaic or subgrain boundaries can be represented by certain arrangements of dislocations. The next obvious step was to devise the experimental techniques for observing dislocations in crystals. A number of techniques were developed and successfully used for revealing the substructure in annealed crystals. These techniques, which included etching, decoration, and various X-ray methods, indicated a general increase in dislocation density after deformation, but were inadequate to reveal the detailed substructure in deformed metals.

The very first observations of subgrains or cell structure in deformed metals were made after straining in creep [51, 52]. The dimensions of these cells were found to depend upon the temperature and the rate of strain; the size of the cells varying from 10 to 100 μm in diameter.

Considerable information regarding the cold-worked structure in metals was gained by using the microbeam X-ray techniques by Hirsch and his co-workers [53-56]. Here, the Debye-Scherrer arcs are no longer found to be continuous, but broken up into spots instead. By counting the number of these spots and examining their shapes, Hirsch and his co-workers were able to study the deformation structure in a number of pure polycrystalline metals, such as Al, Cd, Cu, Fe, Ni, Pb, Sn, and Zn. The results obtained were found to be consistent with the idea that the dislocation distribution in these metals, when deformed, was non-uniform. They concluded that a grain within a cold-worked metal contains a "foam structure" of relatively perfect particles, linked continuously with each other by distorted boundary regions. Thus, the density of dislocations fluctuates from point to point; it is maximum at the particle boundaries and least within the particles. These particles, because of their similarity to the structure observed in creep, were referred to as *cells*, and the particle boundaries as *cell boundaries* or *cell walls*. The cell size, however, was found to be an order of magnitude smaller than that observed in creep. The results of microbeam studies showed that the cell size decreased with increasing impurity content in the metal. It also decreased rapidly during the early stage of deformation and then reached a constant value. This constant value was found to be characteristic of the metal, and was found to increase with the softness of the metal. The microbeam studies further showed that the width of the cell walls increased with the hardness of the metal. All these conclusions drawn from the microbeam experiments were borne out by the extensive

electron microscopic studies carried out later. The average cell size, as determined with the microbeam techniques, is in general found to be larger than that observed by using transmission electron microscopy. However, an excellent agreement has been reported in Al [57].

The results of microbeam techniques were extended further by the development of transmission electron microscopy. In recent years, the deformation structure in a large number of pure fcc metals and alloys have been investigated, and the formation of cell structure in them is found to depend upon several factors; some of them may apply equally well for pure bcc metals and their alloys. It is found that the formation of cell structure is dependent upon the following factors.

(a) *Temperature* The dislocation distribution becomes more uniform, and the tendency of cell formation is reduced when the temperature of deformation is lowered. At higher temperatures, the cell structure is formed at lower strains [28, 35].

(b) *Strain rate* The increase in strain rate is found to have the same effect as lowering the temperature [28].

(c) *Stacking-fault energy* The dislocation distribution becomes more uniform when the stacking-fault energy of the material is reduced. The impurities and the alloying elements tend to alter the stacking-fault energy of the metal, and hence the dislocation distribution [58].

(d) *Precipitates or zones* The size and distribution of precipitates or zones are found to have an important effect in altering the deformation structure. A fine distribution of precipitates can completely suppress cell formation, but large, widely distributed precipitates assist in cell formation [57]. On the other hand, if the fine precipitates are non-uniformly distributed, it is believed that they may also assist cell formation [57].

(e) *Point defects* Interaction of point defects and dislocations has recently been considered by Kuhlmann-Wilsdorf *et al* [59, 60]. Here, the cell formation has been regarded as mainly due to the precipitation of point defects on dislocations. Thus, the presence of a large concentration of point defects is expected to assist cell formation. Experimental results, on the other hand, seem to contradict this; it is found that both in quenched and irradiated metals a higher strain is required for cell formation [61]. It is believed that the distribution of point defects may have a crucial role in determining the dislocation distribution. It has been argued that, while a non-uniform distribution of point defects can assist cell formation, a uniform distribution may prevent it [57].

2.2. Cell Formation

Although a considerable knowledge of the dislocation structure in deformed metals has been gained in the last few years, the precise mechanism of cell formation is still quite obscure. As compared to fcc metals, very little information is available regarding work-hardening of bcc metal single crystals. A number of hardening mechanisms have been proposed for the fcc metals, but they differ considerably from each other [62-65]. The recent deformation studies of bcc single crystals have, however, shown that their work-hardening behaviour is very similar to that of a typical fcc metal [29, 32, 33]. It is, therefore, believed that the basic hardening mechanisms in both fcc and bcc metals are probably the same, except for the obvious crystallographic differences in the slip systems. Recently, a theory of work-hardening of fcc metals has been developed by Hirsch [66], and it is currently believed that the cell formation in bcc metals can be explained equally well on this theory. Although, owing to a lack of experimental data on bcc metals, a quantitative development of the theory has not yet been possible, the cell formation may be explained in a purely intuitive way as follows [32].

Stage I of the work-hardening in bcc crystals resembles closely the "easy glide" of fcc metals, where the dislocations essentially move on their slip planes without encountering obstacles. There is, however, one main difference. While in fcc metals both the edge and screw dislocations traverse large distances, it is only the edge dislocations in bcc metals which move over an appreciable distance. The wavy slip lines observed suggest that during the stage I the screw dislocations mainly move by cross-slip. The electron microscopic studies have also shown a large number of dipoles and elongated dislocation loops, which are believed to be generated by cross-slip of screws. These dipoles can serve as obstacles for dislocation movement, and, as their number is increased, the stress required to push the dislocations through also increases. Stage II begins when the applied

stress, plus the internal stress resolved on the secondary system, is sufficient to activate the secondary sources near the dipoles. Hardening results because of the interaction of the primary and secondary dislocations. In bcc metals, the most significant dislocation reaction is

$$a/2\ [111] + a/2\ [\bar{1}1\bar{1}] = a\ [010] \quad (4)$$

The resultant dislocation is an edge dislocation, which can glide only in a (001) plane which is not a slip plane. In stage II, the dislocations are stopped when they pass close to the regions of high dislocation density, and become a part of the obstacle itself. The obstacles thus become stronger, and their range of interaction increases. Each slip line, therefore, acts as an obstacle for further slip, and the dislocations are clustered. Regions of high dislocation density consisting of primary and secondary dislocations and dipoles trap more dislocations, and an essentially non-uniform distribution of the cell structure is developed during stage II.

Stage III in bcc metals is again similar to that observed in fcc metals. The decrease in work-hardening rate in this stage is considered to be due to the occurrence of cross-slip of screw dislocations. It is suggested that, in bcc metals, either a large-scale cross-slip takes place, or the obstacles are broken [32].

3. Experimental

3.1. Materials

The materials studied were all type II superconductors, and they can be classified in the following three categories: (i) low-κ material – single and polycrystalline Nb; (ii) homogeneous, high-κ material – Nb-50 at. % Ta alloy; and (iii) non-homogeneous, high-field (high-κ) material – Nb-25 at. % Ti and Nb-25 at. % Zr alloys. Of these, the polycrystalline Nb was supplied by Brandhurst, London; while the single crystal was prepared by Metals Research, Cambridge. The Nb alloys were supplied by the International Research and Development Co at Newcastle-upon-Tyne. As a simple test of purity, the resistivity ratio

$$\frac{\rho(300^\circ\ \mathrm{K}) - \rho(4.2^\circ\ \mathrm{K})}{\rho(4.2^\circ\ \mathrm{K})}$$

measured for the polycrystalline Nb specimen was 16; while for the single crystal, it was greater than 400. The alloys, on the other hand, had resistivity ratios less than 10.

Thin foils for transmission electron microscopic examination were prepared either by electropolishing or by chemical polishing; sometimes, a combination of both was followed. The details of the thinning procedures will be reported elsewhere. The specimens were examined in a Siemens Elmiskop 1 microscope operating at 100 kV.

3.2. Superconductivity Measurements

All superconductivity measurements were made at 4.2° K. The specimens were cooled inside a metal cryostat filled with liquid helium. The magnetisation of a specimen was measured directly by moving it axially in or out of search coil, the whole assembly being in a uniform magnetic field parallel to the coil. The change in the magnetic flux was measured by using a sensitive ballistic galvanometer with a lamp and scale. The magnetic field was generated by a superconducting solenoid, wound from Nb-25%Zr alloy wire, which was capable of producing fields up to 45 kOe.

All the critical current measurements reported in this paper were made with the current flowing in the specimen parallel to the applied field. The values of the critical current densities, when the specimen just became normal, were recorded for different magnetic fields. The current measurements on the high-field Nb alloys were made at the Royal Radar Establishment, Malvern, where magnetic fields up to 100 kOe could be produced by using a Bitter solenoid.

4. Results

4.1. Nb

Magnetisation curves of as-received (85 to 90% cold-worked) polycrystalline specimens were highly irreversible, as shown in fig. 2. Optical examination of the etched specimen showed a fibrous structure. Transmission microscopic examination of the specimen revealed a high dislocation density, with dislocations mainly arranged into well-defined cell walls (fig. 2 of reference 25). This material, when annealed for more than 20 h at a temperature close to 2400° C, exhibited a magnetisation behaviour which was almost reversible; the magnetisation curve is also shown in fig. 2. Note the reduction in H_{c_2} due to purification during the anneal. This curve is very similar in shape to Abrikosov's theoretical curve; the value of κ, calculated from the area under the curve and

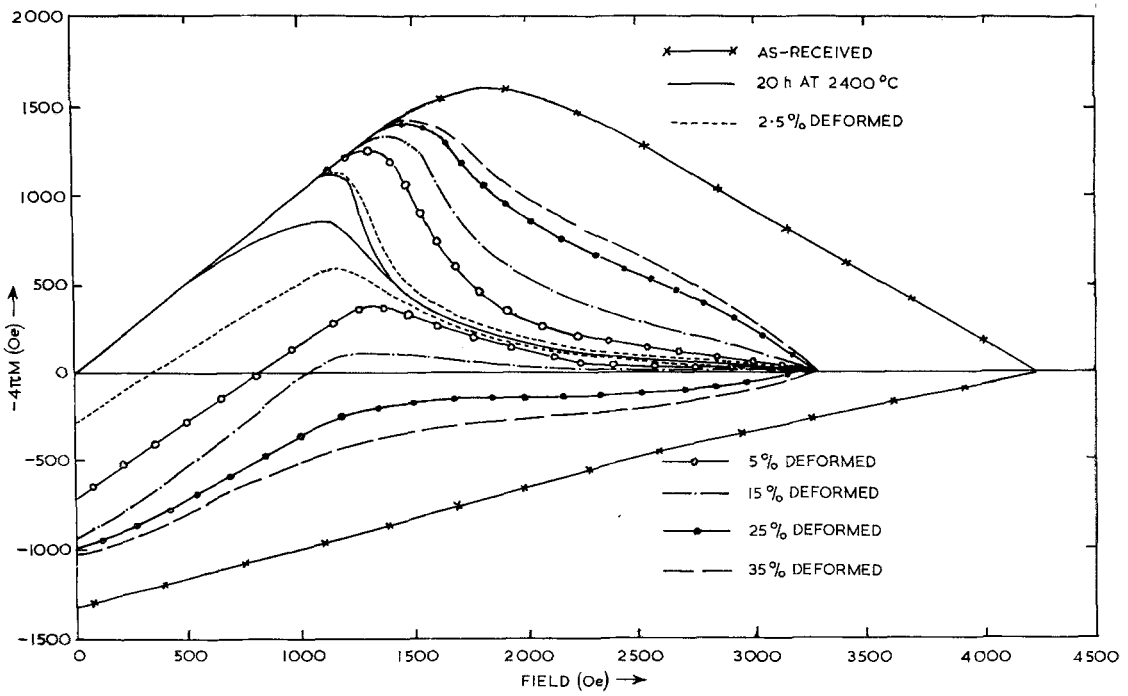

Figure 2 Magnetisation curves of deformed and annealed Nb specimens.

the value of H_{c_2}, was found to be 1.5. The value of H_{c_1}/H_c calculated from Abrikosov's theory [6] was, however, found to differ widely from the value determined from the curve. A similar difficulty was also experienced by Stromberg and Swenson [67], and is due to the fact that the theory is applicable only when $\kappa \gg 1$. Electron microscopic examination of the annealed specimen revealed that it was almost free of dislocations, although some specimen foils did show the presence of a few long dislocations in places. It was not clear whether these dislocations were originally present, or were introduced during preparation of the foils.

The annealed specimen was successively deformed by reducing its thickness by 2.5, 5, 15, 25, and 35%. Magnetisation curves obtained on these specimens show (fig. 2) an increase in hysteresis with deformation. It is now known that the magnetisation of a specimen depends upon its size, and in particular on a composite parameter $a\alpha$ [68, 69]; where a is the radius or the thickness of the specimen, and α is a pinning constant which is a function of the microstructure. For a fixed α, the dependence of the magnetisation upon size is related to the manner in which the pinning force varies with flux line density, and thus in turn will again depend upon the microstructure. In order to determine the correction required in the curves of fig. 2, a detailed study of size effect in Nb and Nb-Ti strips was carried out. Specimens deformed by the same amount but having different final thicknesses were studied, and it was found that the magnetisation in these specimens decreased more slowly than in Pb-Bi alloys [7, 69]. The variation observed was proportional to $a^{\frac{1}{2}}$. A convenient measure of the irreversibility of a superconductor is the *remanent flux*, i.e. the flux trapped as the field is reduced from H_{c_2} to zero. This can be given as a fraction of H_{c_2}: for a completely reversible superconductor, its value is 0; for a completely irreversible superconductor, its value would be 1. Incorporating the correction for the size effect, the values of the remanent flux expressed as fractions of the upper critical field are plotted in fig. 3 against % deformation. This curve is similar to the uncorrected curve (fig. 5 reference 25), except that, after about 10% strain, it does not quite flatten off, but keeps on increasing with deformation, though at a smaller rate.

As may be seen, the increase in remanent flux with deformation is most rapid between 3 and 9% strain; beyond this, it becomes relatively much smaller. The initial rate of increase of remanent flux up to about 3% deformation is

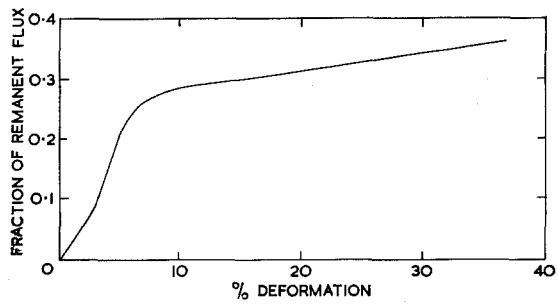

Figure 3 Variation of the fraction of remanent flux with % deformation for Nb specimens.

also low. The dislocation structure introduced in similar specimens deformed by 1, 2, and 3% strains are shown in figs. 4, 5, and 6. The specimen deformed to 1% strain shows a few long dislocations which are mainly screw in character. The dislocations have become kinky and jogs are seen. After deformation to 2%, the specimen shows a general increase in the dislocation density. Also present are a large number of small dislocation loops, which are believed to have been generated by a mechanism involving a double cross-slip of screw dislocations [70]. The general dislocation distribution in the specimen foil is still more or less uniform. Although the dislocations do seem to interact with one another, no isolated dislocation clusters are observed. The first evidence of dislocation tangles is seen in the specimen deformed to 3% strain. The dislocation distribution is no longer completely uniform, for there are now regions present where the dislocation density is higher. Fig. 7 gives the microstructure of a specimen deformed to 5% strain. In most of the regions of the foil, the tangles formed have joined up forming a non-uniform dislocation distribution (cell structure). The concentration of dislocation loops and dipoles in the tangles is higher than within the regions enclosed by the tangles. This suggests that the dipoles and dislocation loops initially generated act as barriers for moving dislocations. Specimens deformed to 10% strain showed a well-developed cell structure (fig. 8). Up to this stage, a slight reduction in the average cell size was occurring with deformation; the average cell size in the 5% deformed specimen decreased from 0.9 μm to a value of 0.7 μm when it was strained to 10%. Further deformation, however, only increased the dislocation density in the cell walls without altering the cell size. The dislocation structures in 14, 35, and 62.5% deformed specimens are shown in figs. 6, 7, and 8 of reference 25.

Summarising: up to initial 3% strain, the increase in remanent flux with deformation is small and dislocations are uniformly distributed. Cell formation begins at about 3% strain and is completed at 10% strain. During this stage, the amount of remanent flux shows its most rapid increase. Once a non-uniform distribution is set up, further deformation makes only a relatively small contribution in enhancing the hysteresis; the dislocation distribution does not change, the new dislocations are merely added to the cell walls making them thicker.

The microstructure and the results of magnetisation measurements of single crystal specimens were essentially identical to the polycrystalline material, and will not be described here. Van Torne and Thomas [30] have argued that cell formation is mainly due to the distribution of impurity precipitates, and that purer materials do not show cell formation. This contradicts the present observations on single crystal specimens, where it was found that the dislocation tangles and the cell structure were produced in an exactly similar manner to that in less pure polycrystalline specimens. This agrees with the work of Fourdeux and Wronski [31], who found that, whereas the load-elongation curve depended markedly upon the purity, the dislocation structure did not. They observed dipoles, tangles, and cell structures in specimens with a resistivity ratio of 118. Their yield stresses were almost half of those found by Van Torne and Thomas; their specimens may be presumed to be of higher purity. The single crystal used in this investigation was of an even higher purity, with a resistivity ratio of >400.

From fig. 2, deformation seems to have no observable effect on the upper critical field. This has been noted also by other workers [71, 72]. Magnetisation measurements are in general not very sensitive methods for measuring H_{c_2}, and it is quite likely that any enhancement which occurred due to deformation may have escaped detection. Critical current measurements made on these materials did, in fact, indicate a slight increase in H_{c_2} after deformation, but these results are not sufficiently definitive to give the increase in κ with increasing dislocation content.

Dislocation structure in Nb specimen.
Figure 4 Deformed 1%.
Figure 5 Deformed 2%.
Figure 6 Deformed 3%.
Figure 7 Deformed 5%.
Figure 8 Deformed 10%.

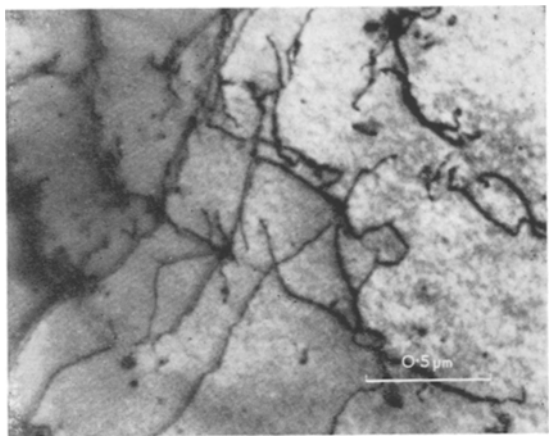

Figure 4

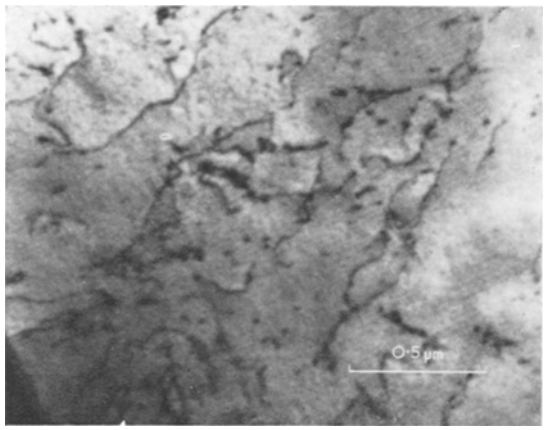

Figure 5

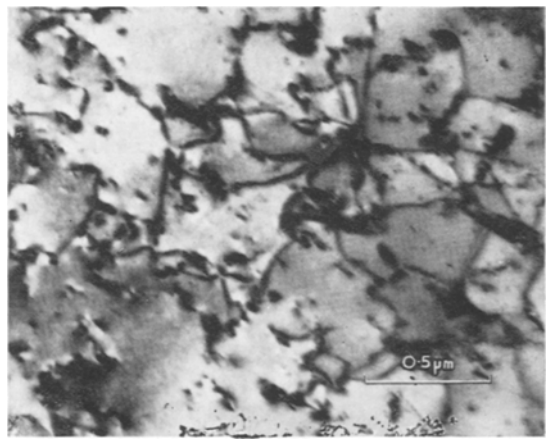

Figure 6

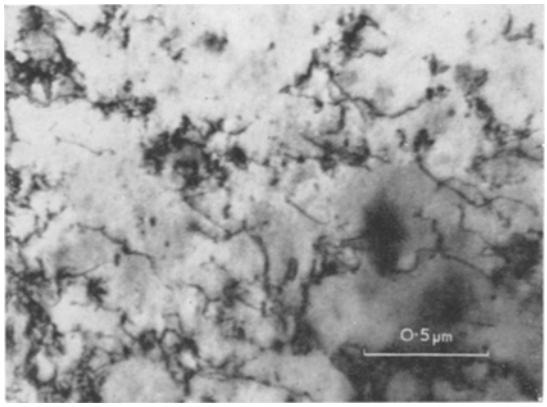

Figure 7

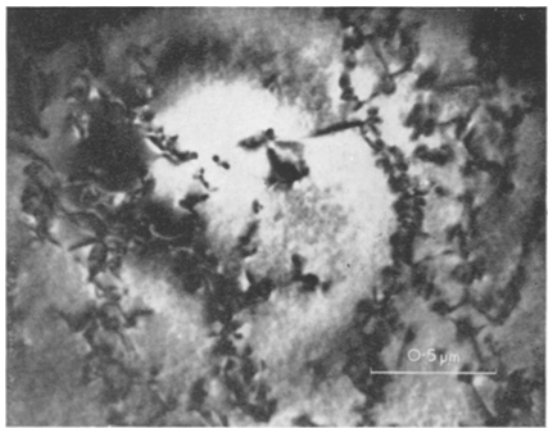

Figure 8

4.3. Nb–50% Ta Alloy

It was mentioned earlier that the value of κ for the material is increased by alloying. Both Nb and Ta have an identical crystal structure and the same lattice spacing (3.3 Å). They form a homogeneous substitutional solid solution over the whole range of composition. By alloying, the periodicity of the lattice potential is broken, and this leads to a decrease in the electron mean free path without distorting the lattice. The alloys of this system have indeed been shown to exhibit an ideal type II behaviour [73]. These alloys have a further advantage in that their upper critical fields are low, being of the order of only a few thousand oersteds, and thus large magnetic fields are not required for their study. A typical dislocation structure observed is shown in fig. 10.

Specimens, when annealed for 4 h at a temperature close to 2400° C in a good vacuum, showed almost completely reversible magnetisation (fig. 9). Thin foils of annealed specimens revealed an absence of dislocations and other defects.

The value of κ as determined from the reversible curve was 5.4, as compared to 1.5 for Nb. The measured value of H_{c1}/H_c was found to be 0.26, and was compared with those calculated from different mixed-state models. Using Abrikosov's theory [6], the ratio was found to be 0.24, while it was 0.36 on the laminar model [74]. This agrees with the results of Harden and Arp [75], who found that the value of H_{c1}/H_c was in better agreement with Abrikosov's theory, and for values of κ less than 20 the deviation from the laminar model was greater than 20%.

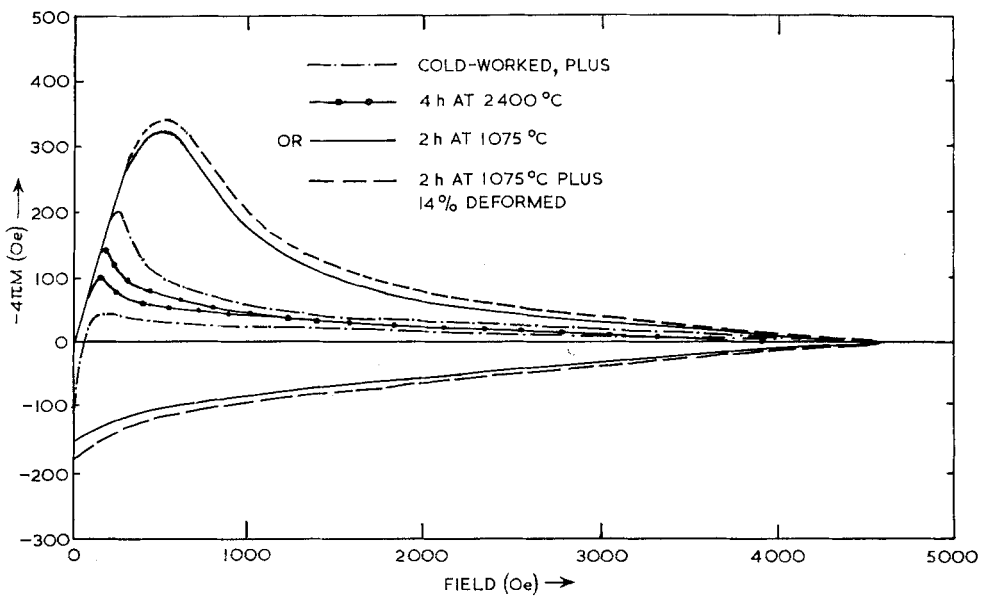

Figure 9 Magnetisation curves of as-received and annealed Nb-Ta specimens.

The magnetisation of an as-received (85 to 90% cold-worked) specimen is shown in fig. 9. The striking feature here is that, compared to the cold-worked Nb specimen, this curve shows much less irreversibility. Transmission electron microscopy of the specimen revealed a high dislocation density, as observed in Nb. The dislocation configuration, however, was quite different; there was no well-defined cell structure, but instead an even distribution of dislocations. The dislocation lines were in general straight, although kinky dislocations were also seen.

The effect of deformation on the annealed specimen was studied, and the magnetisation curves obtained are shown in fig. 11. Qualitatively, the curves are similar to those of Nb, with hysteresis increasing with strain. However, quantitatively, the curves are significantly different; the increase in hysteresis with deformation is comparatively low. The magnitude of

Figure 10 Microstructure in as-received Nb-Ta specimen.

Dislocation structure in 25% deformed Nb-Ta specimen.
Figure 13 Showing elementary cell structure.
Figure 14 Showing uniform dislocation density.

Figure 16 Microstructure in Nb-Ta specimen annealed for 2 h at 1075° C.
Figure 17 As in fig. 16, after 14% deformation.

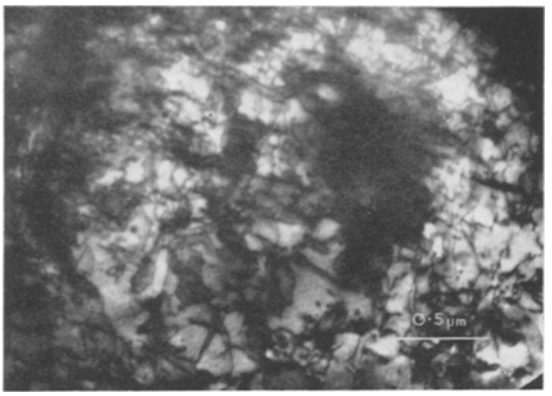

Figure 10

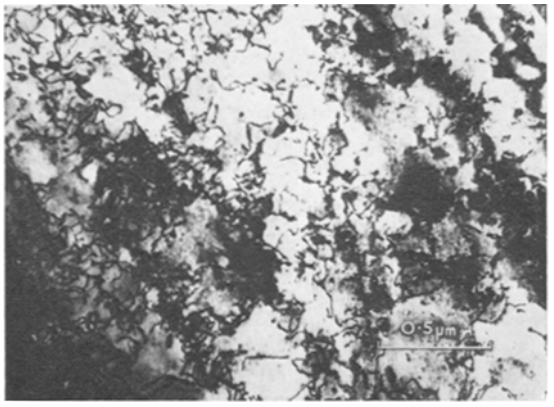

Figure 13

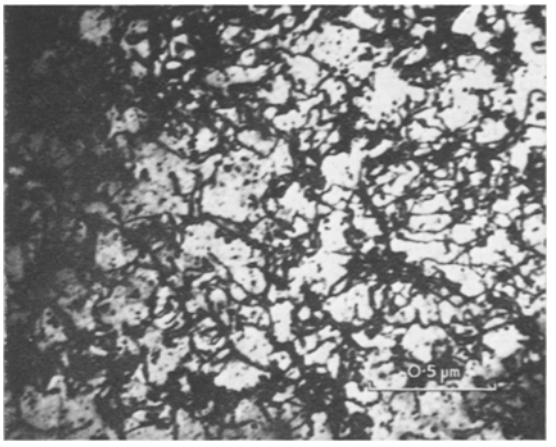

Figure 14

Figure 16

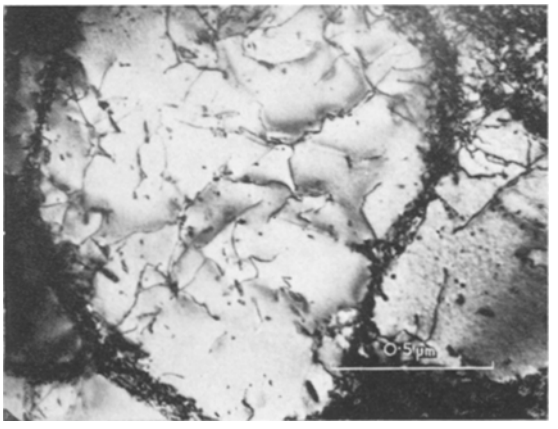

Figure 17

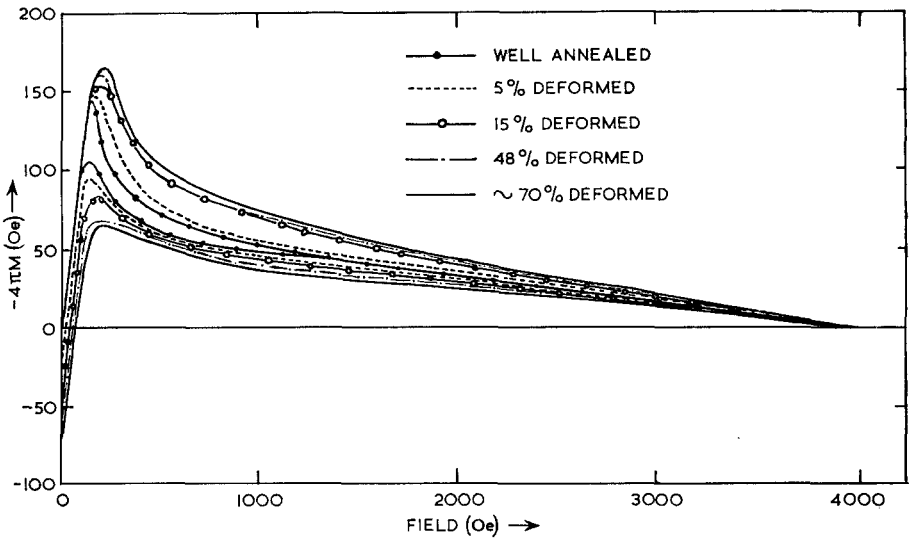

Figure 11 Magnetisation curves of deformed Nb-Ta specimens.

the flux trapped when the applied field is removed is also very small, in all the specimens; it is in fact roughly one-tenth of what was observed in Nb.

Taking into consideration the size effect, the fraction of the remanent flux has been plotted in fig. 12 against the % deformation. The curve, again, is quantitatively quite different from Nb. The kink in the curve, which in Nb had occurred at about 10% strain when the cell structure was developed, now occurs after 20% strain in this alloy.

The microstructure of specimens in various stages of deformation was examined. The dislocation distribution was unlike Nb and was quite uniform. Some evidence of cell formation was noticed only after the specimen was deformed by 25% strain; the cell boundaries were, however, by no means well defined (fig. 13). In most of the regions of the foil, the dislocation distribution was more uniform (fig. 14). Greater amounts of deformation produced no change in dislocation distribution. At all stages of deformation, the presence of a large number of small dislocation loops was observed; their number density was greater, and their size smaller than observed in deformed Nb. A similar effect has been observed in Fe [28], when deformed at low temperatures; it was found that the number density of dislocation loops increased, and their size decreased, and the dislocation distribution became more uniform as the deformation temperature was lowered.

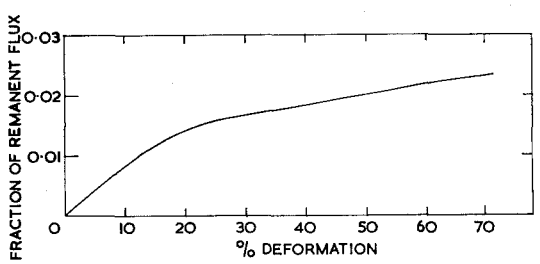

Figure 12 Variation of fraction of remanent flux with % deformation for Nb-Ta specimens.

Fig. 15 shows the results of critical current measurements. A slight increase in H_{c2} after deformation may be noted; this escaped detection in magnetisation measurements.

The cold-worked specimen was then annealed for 2 h at 1075° C, and the magnetisation curve obtained is shown in fig. 9. It is interesting to note that irreversibility and the trapped flux are considerably enhanced after this heat treatment. The microstructure of the specimen is shown in fig. 16. Compared to the cold-worked structure, there has been a considerable reduction in the dislocation *density*. However, more significant is the change in the dislocation *configuration*. The dislocations, which were originally evenly distributed, are now arranged, as a result of polygonisation, into well-defined subboundaries. The dislocation distribution is, therefore, now non-uniform, since there are

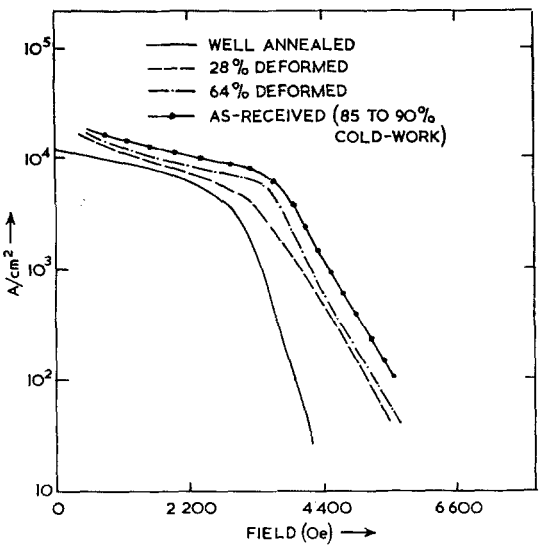

Figure 15 The critical current versus applied field for deformed Nb-Ta alloy.

more dislocations present in the subboundaries than within subgrains.

The effect of deformation on such an annealed specimen was also investigated. The magnetisation curve after 14% deformation is also shown in fig. 9. The two curves are of specimens with the same final thickness. Compared to the unstrained specimen, the 14% deformed specimen shows a small enhancement in hysteresis. The microstructure of this specimen is shown in fig. 17. The regular networks of dislocations are now almost invisible. The subgrains after deformation are still essentially free of dislocations, although some elongated dislocation loops and dipoles are also seen. It is interesting to note that the increase in dislocation density has mainly occurred in the subgrain boundaries, indicating that the networks are the centres of dislocation sources. This result suggests that the current-carrying capacity in certain materials can be improved by suitable intermediate heat treatments during deformation.

4.3. Nb–25% Ti Alloy

According to the Nb-Ti phase diagram [77], alloys containing more than 40 at. % Nb show no phase separation. Consequently, the Nb-25% Ti alloy can be regarded as a single phase material.

Magnetisation of as-received cold-worked material (> 90% deformation) was highly irreversible; the curve obtained is shown in fig. 18. A complete magnetisation curve could not be plotted, because the upper critical field for the specimen (≃ 120 kOe) was much higher than that available in the laboratory. Transmission electron microscopy of the specimen revealed a very high dislocation density with a well-defined cell structure (fig. 19). The average cell size was much smaller than for Nb; the

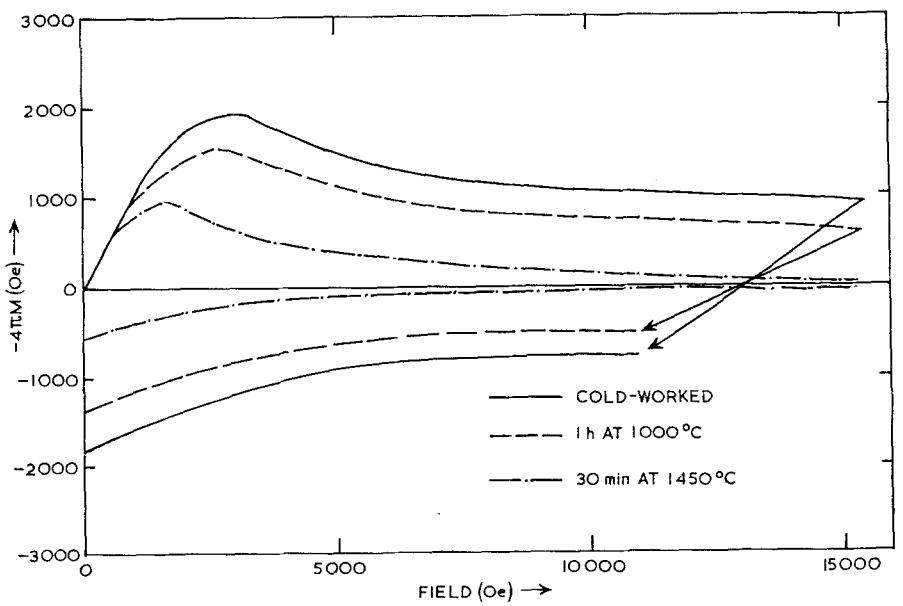

Figure 18 Magnetisation curves of cold-worked and annealed Nb-Ti specimens.

Figure 19 Microstructure in as-received Nb-Ti specimen.

Figure 20 Dislocation structure in Nb-Ti specimen deformed by 2 to 3%.

Dislocation structure in Nb-Ti specimen.
Figure 21 Annealed for 1 h at 1200° C.
Figure 22 Annealed for 30 min at 1450° C.

Figure 26 Microstructure in Nb-Zr specimen annealed for 30 min at 700° C in bad vacuum.

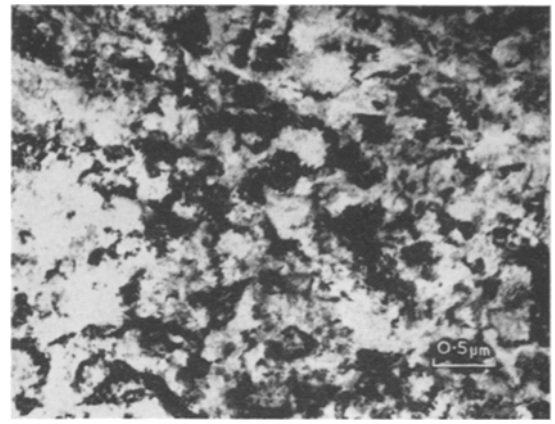

Figure 19

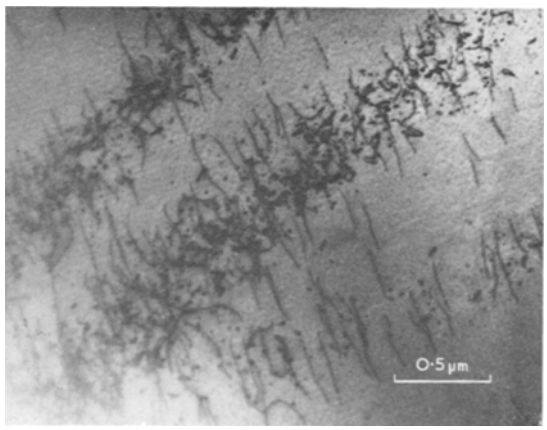

Figure 20

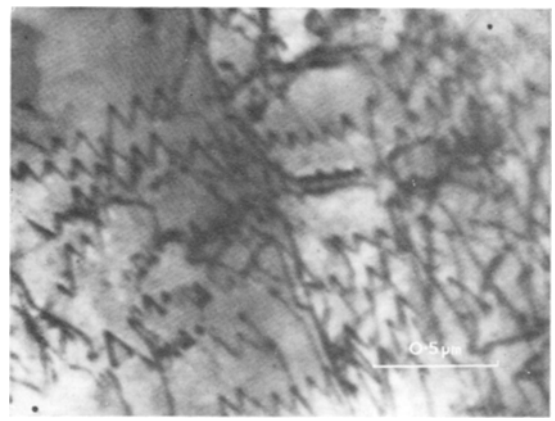

Figure 21

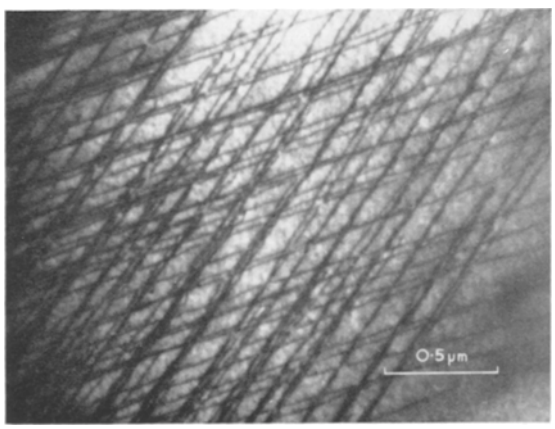

Figure 22

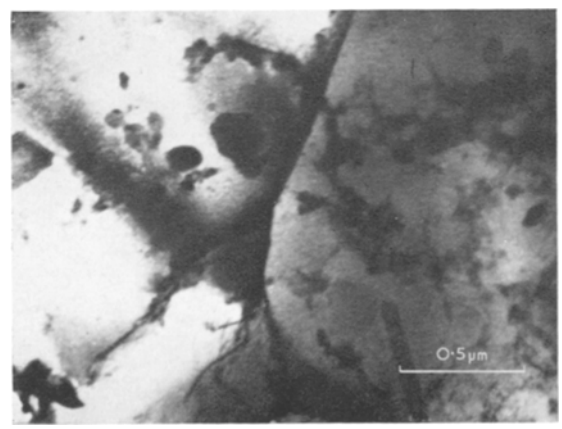

Figure 26

measured value was 0.4 μm, as compared to 0.7 μm for cold-worked Nb.

The effect of deformation on magnetisation of an annealed specimen was not investigated; however, a study of the deformation structure was carried out and was found to be very similar to that of Nb. A specimen deformed 12% showed a well-developed cell structure. An interesting dislocation structure was observed during the early stages of deformation and is shown in fig. 20. Here, the specimen was deformed to 2 to 3% strain. The bands of dislocations essentially consist of screw dislocations and a large number of dipoles and elongated dislocation loops. The picture provides a striking evidence that these loops are generated by the movement of screw dislocations containing jogs. At higher strains, such a structure was replaced by the cell structure.

No significant changes in the microstructure were noted after the cold-worked specimen was annealed for 1 h at 850° C. On increasing the annealing temperature, dislocation interactions began to take place, and as a result dislocations arranged themselves into hexagonal networks. The structures were in no way essentially different from those of Nb-Ta (fig. 16). The magnetisation curve of such a specimen is shown in fig. 18. Compared to the cold-worked specimen, the hysteresis is low. The microstructure in the two specimens differed mainly in two points. First, there was a reduction in dislocation density; second, the cell size increased from 0.4 to about 1μm. The dislocation distribution, however, was still non-uniform.

After annealing for 1 h at 1200° C, the subgrain structure had almost disappeared, and the foil showed regions where the dislocation networks were no longer regular (fig. 21). Annealing for a short time (30 min) at 1450° C resulted in the disappearance of the networks.

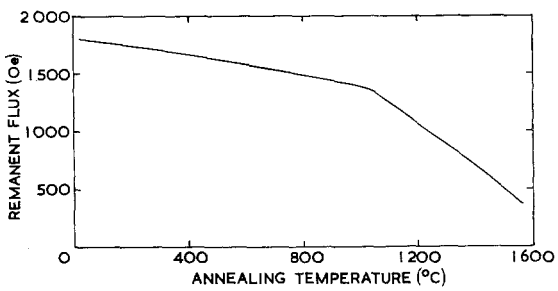

Figure 23 Variation of the remanent flux with annealing temperature for Nb-Ti alloy.

Long and straight dislocations were frequently seen. Fig. 22 shows two intersecting arrays of screw dislocations along $[\bar{1}11]$ and $[11\bar{1}]$ directions lying in a (101) plane. The magnetisation curve of such a specimen is also shown in fig. 18.

Fig. 23 shows the variation of remanent flux with the annealing temperature. The decrease in remanent flux with increasing temperature is slow up to a temperature of 1000° C, and then becomes rapid as the temperature is further increased. Up to about 1000° C, the dislocation distribution is non-uniform; at higher temperatures, the subgrain structure is broken up.

Fig. 24 shows the critical current curves for different annealed specimens.

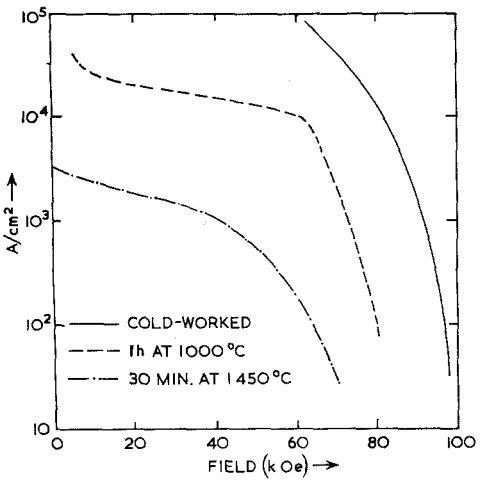

Figure 24 Critical current versus applied field for cold-worked and annealed Nb-Ti specimens.

4.4. Nb–25% Zr Alloy

The phase diagram of the Nb-Zr system [78] contains a monotectoid reaction at 610° C for about 80 at. % of Zr. Berghout [79] has suggested that the monotectoid reaction occurs only in the ternary system Nb-Zr-O, and that in the absence of oxygen the phase diagram is similar to that for Nb-Ti. A number of attempts made to check Berghout's idea have presented contradictory results. On one hand, Walker *et al* [23] have confirmed the original phase diagram of Rogers and Atkins; while on the other hand, the detailed X-ray studies carried out at the International Research and Development Co (Newcastle-upon-Tyne) have failed to detect the two bcc phases in the predicted

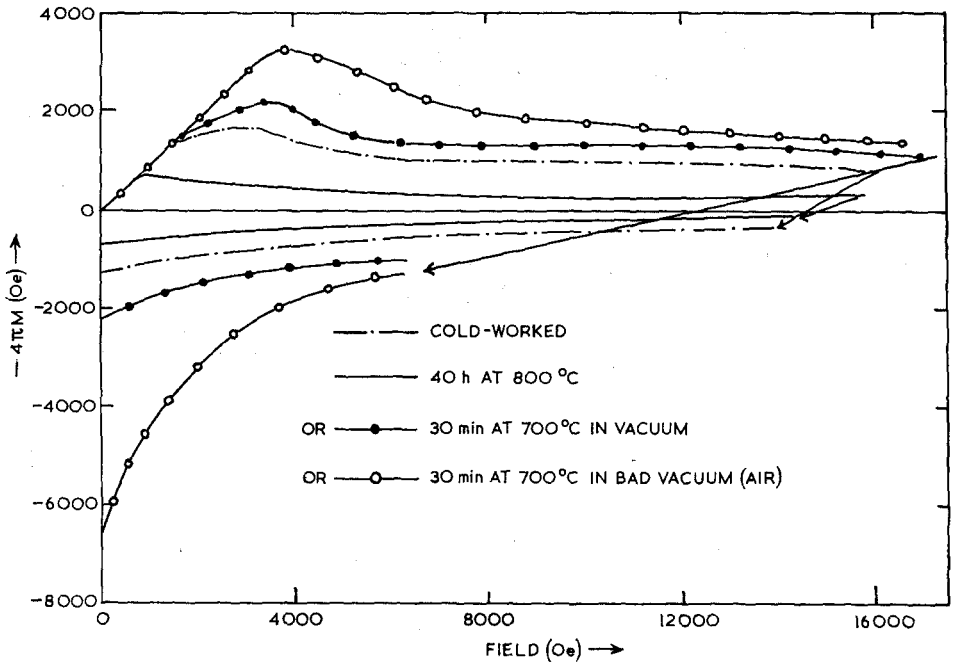

Figure 25 Magnetisation curves of as-received and annealed Nb-Zr specimens.

region, whether the specimen is loaded with oxygen or not [80].

The as-received (cold-worked >90%) specimen showed an irreversible magnetisation behaviour; the curve obtained is shown in fig. 25. The microstructure was identical to that of cold-worked Nb-Ti, but with a cell size fractionally larger at 0.5 μm (cf. 0.4 μm for Nb-Ti). The specimen annealed for 40 h at 800° C showed a very low density of dislocations, with the presence of long dislocations, again similar to Nb-Ti (fig. 22). No precipitation was observed in the specimen. The magnetisation curve obtained also showed a considerable decrease in the hysteresis (fig. 25). However, annealing for a shorter time (30 min) at 700° C enhanced the hysteresis (fig. 25). After this heat treatment, it is believed that a dislocation rearrangement must have occurred to relieve the long-range stresses, the dislocations within the cells have probably moved into the walls, making them more dense. Intermediate anneals during processing of commercial material are reported to improve its current-carrying capacity [80]. The magnetisation of the specimen annealed for 30 min in a bad vacuum was highly irreversible; the curve obtained is also shown in fig. 25. The microstructure in the specimen is shown in fig. 26. The precipitates are believed to be of ZrO_2. The two bcc phases, as predicted by the phase diagram, were never seen in this investigation, but the transformation has been shown to be very sluggish [81].

5. Discussion

No calculation of the direct interaction between one dislocation and one supercurrent vortex has as yet been published. Webb [82] has calculated the interaction between one vortex line and a forest of screw dislocations perpendicular to it; the interaction occurs because of the change in the elastic moduli from the normal core to the superconducting matrix. The interaction is found to be repulsive, and trapping only occurs if the vortex line lies between dislocations. The force per unit length of flux line trapped by a forest of screw dislocations of spacing d is:

$$F_p = -\frac{\Delta S_{44}}{4}\,\frac{(Gb)^2}{d}$$

where G is the shear modulus ($= 1/S_{44}$), b the Burgers vector of the dislocations, and ΔS_{44} the change in S_{44} from normal to superconducting material. The calculation for edge dislocations has not been performed, but will be roughly similar. For a lattice of vortices which are interacting also with one another,

the pinning force should be reduced from the above by about a factor of 10 [83]. Nembach [84] has obtained a uniform dislocation distribution in Nb by torsion, and shown the pinning force to be about one-twentieth of that predicted by Webb. The results reported here on the deformed Nb-Ta alloys indicate that any interaction between uniform dislocation distributions and supercurrent vortices is very small.

Whittam [85] has attempted to measure directly any interaction between vortices and individual dislocations. Stress-strain curves on several alloys of Pb-Bi and Pb-In were measured at 4.2° K in different magnetic fields. Any strong interaction should have resulted in an increased flow stress in the mixed state; this was not observed. A search coil wound closely around the specimen failed to detect any motion of the flux during deformation. If any interaction exists, it must be weak.

All of the evidence presented in this paper is consistent only with a *strong interaction between flux vortices and non-uniform distributions of dislocations*. The normal electron mean free path in a heavily dislocated region will be reduced from the value in a dislocation-free region. This results in an increase in the normal resistivity, and hence an increase in the Ginzburg-Landau parameter κ for such a region (equation 1). It has been suggested [25, 3] that the free energy of a supercurrent vortex is reduced if it lies in a region of higher κ, and that this can account for the observed pinning. This is, however, unlikely to be the correct explanation. The extreme case of a region of different κ is that of a non-superconducting particle. Suppose such a particle exists in the body of an otherwise reversible type II superconductor. In the mixed state, there will be a higher density of vortices passing through the particle than elsewhere in the superconductor (though they will not exist as vortices within the particle), such that the magnetic field in the particle is that in equilibrium with the flux density around it. If extra vortices are now introduced on one side of the particle, some of them will pass into it, displacing others, until equilibrium is again achieved with a uniform, but now higher, flux density throughout the superconductor and a new equilibrium field within the particle. The non-superconducting particle, though it has attached extra vortices to itself, does not act as a barrier to vortex motion.

Pinning by non-superconducting particles must, in fact, be due to the surface barrier to vortex entry which has been shown to exist [86]. Because of the difference in magnetisation between the particle and the superconductor, there must be a circulating supercurrent around the particle. It is this current which interacts with the circulating currents of the vortices. The magnitude of the interaction is proportional to the size of this current, which in turn depends on the difference in equilibrium magnetisation between the particle and the superconductor [7]. For normal Bi particles in a Pb-Bi eutectic, this mechanism has been shown to give the correct pinning force to within an order of magnitude [7, 87]. A normal particle is just a special case of a region of different κ.

For what might be called κ-pinning, the magnitude of the pinning force depends upon three factors. One, the difference in equilibrium magnetisation between the regions with different κ values, $\Delta M(B)$, is a measure of the strength of the surface barrier. This varies with the local value of B within the superconductor, and it has been pointed out [3] that this may in fact change sign at a certain value of B, leading to an unstable regime in the critical current versus applied field curves. The effective pinning of one vortex may also be reduced by the presence of other vortices; this introduces a factor f(B). Finally, there is the microstructural factor which has been shown [7] to be proportional to the total area of the interface, S, between regions of differing κ. The total pinning force is then proportional to $\Delta M(B)\mathrm{f}(B)\, S$. The critical state, mentioned in the introduction, is defined by:

$$\frac{1}{4\pi}\frac{\hat{\phi}_0}{|\phi_0|} \wedge \operatorname{curl} H_A\hat{\phi}_0 = \alpha\, \Delta M(B)\mathrm{f}(B)\, S \qquad (5)$$

where α is a constant, and curl $H_A\hat{\phi}_0$ can be written $\partial H/\partial B$ (curl $B\hat{\phi}_0$). Integration of this equation will give the flux distribution throughout the specimen, and a second integration will give the magnetisation. The boundary condition chosen is that the flux intensity at the surface is in equilibrium with the external field [68]. The critical current can be calculated by adding its self-field to the externally applied field [87].

Equation 5 may be rewritten:

$$\frac{1}{4\pi}\frac{\hat{\phi}_0}{|\phi_0|} \wedge \operatorname{curl} B\,\hat{\phi}_0 = \alpha\, S\, \mathrm{F}(B) \qquad (6)$$

where $F(B) = \Delta M(B)f(B)/m(B)$, and $m(B) = \partial H/\partial B$. This equation cannot be solved without knowing $F(B)$, and in general $F(B)$ is non-analytical. However, an approximate analytic function may be assumed for $F(B)$; for example, if it is taken as being proportional to B^{-n}, then it can be shown [7] that the maximum on the magnetisation curve is proportional to $a^{1/1+n}$, where a is the specimen thickness. Experiments on Nb and Nb-Ti to check this effect give the maximum proportional to $a^{\frac{1}{2}}$, from which it is concluded that $F(B) \propto B^{-2}$. Truly reversible curves were available for none of the specimens, but the curve for annealed Nb in fig. 2 is almost reversible. The slope of this curve is roughly proportional to B^{-1} in the region just above H_{c1}.

$f(B)$ is the reduction in pinning due to more than one vortex at a pinning point. The mixed state in Nb commences at about 1000 Oe, this corresponds to a vortex spacing ($\phi_0 = 2 \times 10^{-7}$ gauss/cm^2) of about 0.1 μm, which is much less than the observed cell size (0.7 μm for 10% deformation). Each cell wall will, therefore, be pinning several vortices, and Evetts [7] has shown that in this case $f(B)$ should be proportional to $B^{-\frac{1}{2}}$. $\Delta M(B)$ must, therefore, also be proportional to $B^{-\frac{1}{2}}$. $\Delta M(B)$ is the difference in reversible magnetisation between the superconducting matrix and the defects responsible for pinning, in this case the dislocation tangles. κ for the tangles is not known, but a variation of $\Delta M(B) \propto B^{-\frac{1}{2}}$ is entirely reasonable. A similar analysis is not possible for the alloys, but there is no reason to suppose that they are very different, except for the magnitude of the effects involved, from pure Nb.

It may be concluded that the hysteresis and high current-carrying capacity of deformed type II superconductors are due to non-uniform distribution of dislocations. Dislocation tangles form regions with superconducting properties which differ from those of the matrix. The magnitude of the effects is proportional to the extent of the difference in superconducting properties $\Delta M(B)$ and to the total surface area of these regions (S). The first may be increased by increasing dislocation density in the tangles, by either increased cold-work or by precipitation upon them. The second is increased by decreasing the scale of the cell structure; this is a characteristic of the particular alloy, but may be decreased by an increase in stacking fault energy or by controlling the temperature of deformation.

Acknowledgements

This work was financially supported by the Central Electricity Generating Board. The authors are indebted to their colleagues A. M. Campbell, J. E. Evetts, and M. Whittam, for much discussion and for access to unpublished results. They are grateful to Professor A. H. Cottrell and the Department of Metallurgy at Cambridge, and to the Ministry of Aviation and the Director of the Royal Radar Establishment, for the provision of experimental facilities. One of us (A.V.N.) wishes to thank the governing body of Peterhouse, and latterly the Central Electricity Generating Board, for the award of a research studentship. This paper is based in part on a dissertation submitted by A. V. Narlikar for the Ph.D. degree at Cambridge.

References

1. J. D. LIVINGSTON and H. W. SCHADLER, *Prog. Mat. Science* **12** (1965) 183.
2. J. A. CATTERALL, *Metallurgical Reviews* **11** (1966) 25.
3. D. DEW-HUGHES, *Materials Science and Engineering* **1** (1966) 2.
4. V. L. GINZBURG and L. D. LANDAU, *Zh. Eksp. Teor. Fiz.* **20** (1950) 1064.
5. B. B. GOODMAN, *IBM J. Res. Develop.* **6** (1962) 63.
6. A. A. ABRIKOSOV, *Soviet Phys. JETP* **5** (1957) 1174.
7. J. E. EVETTS, Ph.D. thesis, Cambridge (1966).
8. C. F. HEMPSTEAD and Y. B. KIM, *Phys. Rev. Letters* **12** (1964) 145.
9. W. F. DRUYVESTEYN and J. VOLGER, *Philips Res. Reports* **9** (1964) 149.
10. R. G. JONES, E. H. RHODERICK, and A. C. ROSE-INNES, *Phys. Letters* **15** (1965) 214.
11. H. O. LORCH, *Phys. Letters* **17** (1965) 196.
12. B. D. JOSEPHSON, *Phys. Letters* **16** (1965) 242.
13. H. G. B. CASIMIR, *Phys. Letters* **17** (1965) 177.
14. J. G. PARK, *Phys. Letters* **20** (1966) 346.
15. R. H. ROMER, *Phys. Letters* **17** (1965) 223.
16. B. B. GOODMAN and M. R. WERTHEIMER, *Phys. Letters* **18** (1965) 236.
17. M. R. WERTHEIMER, B. B. GOODMAN, and A. LACAZE, Motion Picture of Flux Motion, presented at Solid State Physics Conf., Manchester (1966).
18. J. W. HEATON and A. C. ROSE-INNES, *Cryogenics* **4** (1964) 85.
19. R. W. SHAW and D. E. MAPOTHER, *Phys. Rev.* **118** (1960) 1474.
20. J. J. HAUSER and E. BUEHLER, *Phys. Rev.* **125** (1962) 142.
21. J. J. HAUSER and E. HELFAND, *Phys. Rev.* **127** (1962) 386.
22. J. A. CATTERALL, I. WILLIAMS, and J. F. DUKE, *Brit. J. Appl. Phys.* **15** (1964) 1369.

23. M. S. WALKER, R. STICKLER, and F. E. WERNER, "Metallurgy of Advanced Electronic Materials", edited by G. E. Brock (Interscience, New York, 1962), p. 49.
24. I. WILLIAMS and J. A. CATTERALL, *Brit. J. Appl. Phys.* **17** (1966) 505.
25. A. V. NARLIKAR and D. DEW-HUGHES, *Phys. stat. solidi* **6** (1964) 383.
26. G. J. VAN GURP and D. J. VAN OOIJEN, paper presented at the Colloque sur la Physique des Dislocations, Toulouse (March 1966).
27. A. S. KEH, "Direct Observations of Imperfections in Crystals" (Interscience, New York, 1962), p. 213.
28. A. S. KEH and S. WEISSMANN, "Electron Microscopy and Strength of Crystals" (Interscience, New York, 1963), p. 231.
29. A. S. KEH, *Phil. Mag.* **12** (1965) 9.
30. L. I. VAN TORNE and G. THOMAS, *Acta Met.* **11** (1963) 881.
31. A. FOURDEUX and A. WRONSKI, *J. Less-Common Met.* **7** (1964) 205.
32. T. E. MITCHELL, R. A. FOXALL, and P. B. HIRSCH, *Phil. Mag.* **8** (1963) 1895.
33. T. E. MITCHELL and W. A. SPITZIG, *Acta Met.* **13** (1965) 1169.
34. *Idem*, to be published.
35. J. W. EDDINGTON and R. E. SMALLMAN, *Acta Met.* **12** (1964) 1313.
36. J. W. EDDINGTON, T. C. LINDLEY, and R. E. SMALLMAN, *ibid*, 1025.
37. R. BENSON, G. THOMAS, and J. WASHBURN, "Direct Observations of Imperfections in Crystals" (Interscience, New York, 1962), p. 375.
38. F. O. JONES, "Niobium, Tantalum, Molybdenum and Tungsten" (Elsevier, 1961), p. 158.
39. Y. NAKAYAMA, S. WEISSMANN, and T. IMURA, "Direct Observation of Imperfections in Crystals" (Interscience, New York, 1962), p. 573.
40. A. WRONSKI and A. FOURDEUX, *Phil. Mag.* **10** (1964) 969.
41. L. I. VAN TORNE and G. THOMAS, *Acta Met.* **14** (1966) 621.
42. R. D. HEIDENREICH, *J. Appl. Phys.* **20** (1949) 993.
43. C. G. DARWIN, *Phil. Mag.* **43** (1922) 800.
44. L. G. PARRATT, *Phys. Rev.* **41** (1932) 561.
45. M. RENNINGER, *Z. Krist.* **89** (1934) 344.
46. R. W. JAMES, *ibid*, 295.
47. A. SMEKAL, *Handbuch der Physik* **24** (1933) 795.
48. F. ZWICKY, *Physik. Z.* **24** (1923) 131.
49. W. L. BRAGG, *Proc. Phys. Soc.* **52** (1940) 54.
50. J. M. BURGERS, *ibid*, 23.
51. W. A. WOOD and G. R. WILMS, *J. Inst. Met.* **75** (1948) 693.
52. D. MCLEAN, *J. Inst. Met.* **80** (1951) 507.
53. P. GAY and A. KELLY, *Acta Cryst.* **6** (1953) 165.
54. *Idem, ibid*, 172.
55. P. GAY, P. B. HIRSCH, and A. KELLY, *Acta Cryst.* **7** (1954) 41.
56. A. KELLY, *ibid*, 554.
57. P. R. SWANN, "Electron Microscopy and Strength of Crystals" (Interscience, New York, 1963), p. 131.
58. A. HOWIE, "Direct Observations of Imperfections in Crystals" (Interscience, New York, 1962), p. 283.
59. H. G. F. WILSDORF and D. KUHLMANN-WILSDORF, *Phys. Rev. Letters* **3** (1959) 170.
60. D. KUHLMANN-WILSDORF and H. G. F. WILSDORF, "Electron Microscopy and Strength of Crystals" (Interscience, New York, 1963), p. 575.
61. I. G. GREENFIELD and H. G. F. WILSDORF, *J. Appl. Phys.* **32** (1961) 827.
62. A. SEEGER, "Dislocations and Mechanical Properties of Crystals" (Wiley, New York, 1957), p. 243.
63. Z. S. BASINSKI, *Phil. Mag.* **4** (1959) 393.
64. N. F. MOTT, *Trans. AIME* **218** (1960) 962.
65. P. B. HIRSCH, *Phil. Mag.* **7** (1962) 67.
66. *Idem*, Discussions of the Faraday Society No. 38, The Faraday Society, London (1964) 111.
67. T. F. STROMBERG and C. A. SWENSON, *Phys. Rev. Letters* **9** (1962) 370.
68. A. M. CAMPBELL, J. E. EVETTS, and D. DEW-HUGHES, *Phil. Mag.* **10** (1964) 333.
69. J. E. EVETTS, D. DEW-HUGHES, and A. M. CAMPBELL, *Phys. Letters* **16** (1965) 113.
70. J. WASHBURN, G. W. GROVES, A. KELLY, and G. K. WILLIAMSON, *Phil. Mag.* **5** (1960) 991.
71. J. D. LIVINGSTON, *Phys. Rev.* **129** (1963) 1943.
72. A. ECHARRI, Ph.D. thesis, University of Grenoble (1966).
73. A. CALVERLEY and A. C. ROSE-INNES, *Proc. Roy. Soc.* **A225** (1960) 267.
74. B. B. GOODMAN, *Phys. Rev. Letters* **6** (1961) 597.
75. V. L. HARDEN and V. ARP, *Cryogenics* **3** (1963) 105.
76. Deleted in proof.
77. M. HANSEN, "The Constitution of Binary Alloys" (McGraw Hill, New York, 1958), p. 1019.
78. B. A. ROGERS and D. F. ATKINS, *Trans. AIME* **203** (1955) 1034.
79. C. W. BERGHOUT, *Phys. Letters* **1** (1962) 292.
80. Discussion on Metallurgy of High-Field Superconductors, London (1964).
81. G. R. LOVE and M. L. PICKLESIMER, *Trans. AIME* **236** (1966) 430.
82. W. W. WEBB, *Phys. Rev. Letters* **11** (1963) 191.
83. R. LABUSCH, quoted in reference 26.
84. E. NEMBACH, *Phys. stat. solidi* **13** (1966) 543.
85. M. WHITTAM, M.Sc. thesis, University of Lancaster (1965).
86. C. P. BEAN and J. D. LIVINGSTON, *Phys. Rev. Letters* **12** (1964) 14.
87. A. M. CAMPBELL, Ph. D. thesis, Cambridge (1966).